CERN-TH-2016-215, LTH 1104, OUTP-16-23P

Constraints on the trilinear Higgs coupling from vector boson fusion and associated Higgs production at the LHC

Wojciech Bizoń,[1] **Martin Gorbahn,**[2] **Ulrich Haisch**[1,3] **and Giulia Zanderighi**[1,3]

[1] *Rudolf Peierls Centre for Theoretical Physics, University of Oxford, OX1 3NP Oxford, United Kingdom*

[2] *Department of Mathematical Sciences, University of Liverpool, L69 7ZL Liverpool, United Kingdom*

[3] *CERN, Theoretical Physics Department, CH-1211 Geneva 23, Switzerland*

E-mail: Wojciech.Bizon@physics.ox.ac.uk, Martin.Gorbahn@liverpool.ac.uk, Ulrich.Haisch@physics.ox.ac.uk, Giulia.Zanderighi@physics.ox.ac.uk

We examine the constraints on the trilinear Higgs coupling λ that originate from associated (Vh) and vector boson fusion (VBF) Higgs production in pp collisions in the context of the Standard Model effective field theory. The 1-loop contributions to $pp \to Vh$ and $pp \to jjh$ that stem from insertions of the dimension-6 operator $O_6 = -\lambda \left(H^\dagger H\right)^3$ are calculated and combined with the $\mathcal{O}(\lambda)$ corrections to the partial decay widths of the Higgs boson. Employing next-to-next-to-leading order QCD predictions, we analyse the sensitivity of current and forthcoming measurements of the signal strengths in Vh and VBF Higgs production to changes in λ. We show that future LHC runs may be able to probe modifications of λ with a sensitivity similar to the one that is expected to arise from determinations of double-Higgs production. The sensitivity of differential Vh and VBF Higgs distributions to a modified h^3 coupling is also studied.

Contents

1 Introduction

Within the Standard Model (SM), the mass and the self-interactions of the Higgs field h are parametrised by the potential

$$\mathcal{L}_{\rm SM} \supset -V_{\rm SM} = -\frac{m_h^2}{2}\,h^2 - \lambda v\, h^3 - \frac{\kappa}{4}\,h^4\,, \tag{1.1}$$

where $v = 246.22\,\text{GeV}$ denotes the Higgs vacuum expectation value and

$$\lambda = \kappa = \frac{m_h^2}{2v^2}\,. \tag{1.2}$$

The LHC measurement of the Higgs-boson mass $m_h = 125.09\,\text{GeV}$ [1] determined the first term in (1.1), but the h^3 and h^4 couplings, and in particular the SM relation (1.2) have not been tested. Trying to constrain the Higgs self-couplings and thereby exploring the mechanism of electroweak symmetry breaking (EWSB) is hence an important goal of forthcoming LHC runs and other future high-energy colliders such as a hadron-hadron Future Circular Collider or a Circular Electron-Positron Collider.

One way to constrain the coefficients λ and κ in (1.1) consists in measuring double-Higgs and triple-Higgs production. Since the cross section for $pp \to 3h$ production is of $\mathcal{O}(0.1\,\text{fb})$

at 14 TeV centre-of-mass energy ($\sqrt{s}$) even the high-luminosity option of the LHC (HL-LHC) will only be able to set very loose bounds on the Higgs quartic. The prospect to observe double-Higgs production at the HL-LHC is considerably better because at 14 TeV the $pp \to hh$ production cross section amounts to $\mathcal{O}(35\,\text{fb})$ [2–9]. Measuring double-Higgs production at the HL-LHC however still remains challenging (see for instance [10–27]) and as a result even with the full data set of $3\,\text{ab}^{-1}$ only an $\mathcal{O}(1)$ determination of the trilinear Higgs coupling seems possible under optimistic assumptions.

A second possibility consists in studying the effects that a modification of λ has at loop level in single-Higgs production. In fact, such indirect probes of the h^3 coupling have been first proposed in the context precision studies of $e^+e^- \to hZ$ [28, 29] and subsequently extended to observables accessible at hadronic machines such as the LHC [30, 31]. For both types of colliders it has been shown that future determination of λ via loop effects are complementary to the direct HL-LHC determination through $pp \to hh$, since these probes can provide competitive constraints under the simplified assumption that new-physics effects dominantly modify the h^3 coupling.

This paper is a sequel to the article [30], in which two of us have calculated the $\mathcal{O}(\lambda)$ corrections to the $gg \to h$ and $h \to \gamma\gamma$ processes that arise at the 2-loop level within the SM effective field theory (SMEFT). The discussion in the present paper focuses instead on associated (Vh) and vector boson fusion (VBF) Higgs production. Specifically, we compute the 1-loop contributions to the $pp \to Vh$ and $pp \to jjh$ amplitudes that result from insertions of the effective operator $O_6 = -\lambda \left(H^\dagger H\right)^3$. Combining these contributions with the $\mathcal{O}(\lambda)$ corrections to the partial decay widths of the Higgs boson, we analyse the sensitivity of present and future LHC measurements of the Vh and VBF Higgs processes to shifts in the trilinear Higgs interactions. In order to obtain high-precision predictions for the Vh and VBF Higgs cross sections we include QCD corrections up to next-to-next-to-leading order (NNLO) in our study. We find that HL-LHC measurements of the Vh and VBF signal strengths may allow to set bounds on the Wilson coefficient of O_6 that are comparable to the limits that are expected to arise from HL-LHC determinations of $pp \to hh$. By studying differential distributions it may even be possible to improve the obtained constraints. We present NNLO predictions for the Vh and VBF Higgs distributions that are most sensitive to the shifts in the trilinear Higgs interactions. Our analysis shows that measurements of the spectra in Vh production provide sensitivity to the relative sign of the Wilson coefficient of O_6. The discriminating power in VBF Higgs production is less pronounced compared to the Vh channels. A similar investigation of the Vh and VBF Higgs processes in an anomalous coupling approach was presented in [31]. Whenever indicated we will highlight the similarities and differences between this and our work.

The article at hand is structured in the following way. In Section 2 we introduce the effective interactions relevant for the computations performed in our paper. The results of our loop calculations of the VVh vertex and the partial decay widths of the Higgs boson are presented in Section 3 and 4, respectively. The computations of the vector boson mediated Higgs cross sections and distributions are described in Section 5 and 6. Our numerical analysis is presented in Section 7. Both LHC Run I and HL-LHC constraints on the trilinear Higgs coupling are considered. Section 8 contains our conclusions.

2 Preliminaries

Physics beyond the SM (BSM) can be described in a model-independent fashion by supplementing the SM Lagrangian $\mathcal{L}_{\rm SM}$ by effective operators O_k of mass dimension six. In our article, we will consider the following Lagrangian

$$\mathcal{L} = \mathcal{L}_{\rm SM} + \sum_{k=6,H} \frac{\bar{c}_k}{v^2} O_k \,, \tag{2.1}$$

where

$$O_6 = -\lambda \left(H^\dagger H\right)^3 , \qquad O_H = \frac{1}{2} \partial_\mu \left(H^\dagger H\right) \partial^\mu \left(H^\dagger H\right) , \tag{2.2}$$

with λ defined as in (1.2) and H denoting the SM Higgs doublet. The dimension-6 operators introduced in (2.2) modify the trilinear Higgs coupling. Upon canonical normalisation of the Higgs kinetic term, one finds

$$\mathcal{L} \supset -\lambda c_3 v h^3 = -\lambda \left(1 + \bar{c}_6 - \frac{3\bar{c}_H}{2}\right) v h^3 \,, \tag{2.3}$$

where the Wilson coefficients $\bar{c}_6$ and $\bar{c}_H$ as well as the trilinear Higgs coupling λ are all understood to be evaluated at the weak scale hereafter denoted by μ_w.

It is important to realise that the indirect probes of the trilinear Higgs coupling considered in our work measure c_3, i.e. the coefficient multiplying the interaction term $-\lambda v h^3$ in the effective Higgs potential after EWSB. Relating the coefficient c_3 to any underlying theory, such as for instance the SMEFT, necessarily involves model assumptions. In the following we will focus our attention on BSM scenarios where the Wilson coefficient $\bar{c}_6$ represents the only relevant modification of the h^3 vertex. Corrections due to $\bar{c}_H$ are on the other hand ignored. Such effects will cause a universal shift in all Higgs-boson couplings at tree level and also induce logarithmically-enhanced contributions to the oblique parameters S and T at the 1-loop level [32]. The Wilson coefficient $\bar{c}_H$ can therefore be probed by means other than Vh or VBF Higgs production that are the focal point of the present work. We also do not consider effects of dimension-8 operators such as $-\lambda \bar{c}_8/v^4 \left(H^\dagger H\right)^4$.[1] Under these model assumptions one obtains the simple relation

$$c_3 = 1 + \bar{c}_6 \,, \tag{2.4}$$

which allows one to parameterise modifications of the h^3 vertex in terms of the Wilson coefficient $\bar{c}_6$. In our article we will use this parameterisation, but emphasise that all formulas and results presented in the following sections can be translated to an anomalous coupling approach by simply replacing $\bar{c}_6$ with $c_3 - 1$. In fact, we have verified that to the perturbative order considered here and in [31] the calculations of Vh and VBF Higgs production in the SMEFT and the anomalous coupling framework agree exactly if the relation (2.4) is taken into account.

[1] The effects of $-\lambda \bar{c}_8/v^4 \left(H^\dagger H\right)^4$ could be easily incorporated in our analysis by shifting the coefficient c_3 introduced in (2.3) by $2\bar{c}_8$ [30].

3 Corrections to the VVh vertex

In the SMEFT there can be two different types of corrections to the VVh vertex with $V = W, Z$. First, terms that are enhanced by logarithms of the form $\ln(\Lambda^2/\mu_w^2)$ which are associated to the renormalisation group evolution that connects the new-physics scale Λ to μ_w and second, finite contributions that originate from the corrections to the VVh Green's function with a modified h^3 vertex. Since the operator O_6 only mixes with itself at the 1-loop level [33–36], the VVh vertex does not receive logarithmically-enhanced corrections proportional to $\bar{c}_6$ at the first non-trivial order in perturbation theory.

The full $\mathcal{O}(\lambda)$ corrections to the renormalised VVh vertex thus arise from the 1-loop diagrams shown in Figure 1 and a tree-level counterterm graph involving a Higgs wave function renormalisation. We determine the relevant contributions using `FeynArts` [37] and `FormCalc` [38]. Including the SM tree-level contribution, our final result for the renormalised VVh vertex reads

$$\Gamma_V^{\mu\nu}(q_1, q_2) = 2\left(\sqrt{2}G_F\right)^{1/2} m_V^2 \left[\eta^{\mu\nu}\left(1 + \mathcal{F}_1(q_1^2, q_2^2)\right) + q_1^\nu q_2^\mu\, \mathcal{F}_2(q_1^2, q_2^2)\right], \tag{3.1}$$

where $G_F = 1/(\sqrt{2}v^2)$ is the Fermi constant, $\eta^{\mu\nu}$ is the metric tensor, while m_V and q_i^μ with $i = 1, 2$ denote the mass and the 4-momenta of the external gauge bosons. The indices and momenta are assigned to the vertex as $V^\mu(q_1) + V^\nu(q_2) \to h(q_1 + q_2)$ with $(q_1 + q_2)^2 = m_h^2$, i.e. an on-shell Higgs boson. Notice that $\Gamma_V^{\mu\nu}(q_1, q_2)$ contains only Lorentz structures that gives rise to a non-vanishing contribution when the vertex is contracted with massless fermion lines, which is equivalent to including only transversal gauge-boson polarisations $\varepsilon_i^\mu(q_i)$ in an on-shell calculation by requiring $\varepsilon_i(q_i) \cdot q_i = 0$.

The form factors entering (3.1) can be expressed in terms of the following 1-loop Passarino-Veltman (PV) scalar integrals

$$\begin{aligned}
B_0\big(p_1^2, m_0^2, m_1^2\big) &= \frac{\mu^{4-d}}{i\pi^{d/2} r_\Gamma} \int \frac{d^d l}{\prod_{i=0,1} P(l + p_i, m_i)}\,, \\
B_0'\big(p_1^2, m_0^2, m_1^2\big) &= \left.\frac{\partial B_0\big(k^2, m_0^2, m_1^2\big)}{\partial k^2}\right|_{k^2 = p_1^2}\,, \\
C_0\big(p_1^2, (p_1 - p_2)^2, p_2^2, m_0^2, m_1^2, m_2^2\big) &= \frac{\mu^{4-d}}{i\pi^{d/2} r_\Gamma} \int \frac{d^d l}{\prod_{i=0,1,2} P(l + p_i, m_i)}\,,
\end{aligned} \tag{3.2}$$

and the tensor coefficients of the two tensor integrals

$$\begin{aligned}
C^\mu\big(p_1^2, (p_1 - p_2)^2, p_2^2, m_0^2, m_1^2, m_2^2\big) &= \frac{\mu^{4-d}}{i\pi^{d/2} r_\Gamma} \int \frac{d^d l\; l^\mu}{\prod_{i=0,1,2} P(l + p_i, m_i)}\,, \\
C^{\mu\nu}\big(p_1^2, (p_1 - p_2)^2, p_2^2, m_0^2, m_1^2, m_2^2\big) &= \frac{\mu^{4-d}}{i\pi^{d/2} r_\Gamma} \int \frac{d^d l\; l^\mu l^\nu}{\prod_{i=0,1,2} P(l + p_i, m_i)}\,.
\end{aligned} \tag{3.3}$$

Here μ is the renormalisation scale that keeps track of the correct dimension of the integrals in $d = 4 - 2\epsilon$ space-time dimensions, $r_\Gamma = \Gamma^2(1 - \epsilon)\Gamma(1 + \epsilon)/\Gamma(1 - 2\epsilon)$ with $\Gamma(z)$ denoting

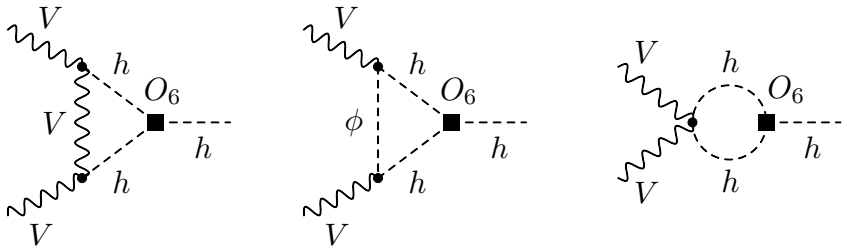

Figure 1. The three 1-loop diagrams with an insertion of the effective operator O_6 that contribute to the VVh vertex at $\mathcal{O}(\lambda)$. Here ϕ denotes the relevant would-be Goldstone field that needs to be included if the calculation is performed in a R_ξ gauge.

the Euler gamma function, $P(k,m) = k^2 - m^2$ and $p_0 = 0$. The definitions (3.2) and (3.3) resemble those of the `LoopTools` package [38].

The integrals with a tensor structure (3.3) can be reduced to linear combinations of Lorentz-contravariant tensors constructed from the metric tensor $\eta^{\mu\nu}$ and a linearly independent set of the 4-momenta p_i^μ. We define the tensor coefficients of the triangle integrals in the following way

$$C^\mu = \sum_{i=1,2} p_i^\mu C_i \,, \qquad C^{\mu\nu} = \eta^{\mu\nu} C_{00} + \sum_{i,j=1,2} p_i^\mu p_j^\nu C_{ij} \,. \tag{3.4}$$

Notice that of all scalar and tensor-coefficient functions appearing in our 1-loop calculations only B_0 and C_{00} are ultraviolet (UV) divergent. These divergent contributions appear in our final results always in the UV-finite combination $B_0 - 4C_{00}$.

With the definitions (3.2), (3.3) and (3.4) at hand, the full analytic expressions of the form factors can be written as

$$\begin{aligned} \mathcal{F}_1(q_1^2, q_2^2) &= \frac{\lambda \bar{c}_6}{(4\pi)^2} \left(-3B_0 - 12\left(m_V^2 C_0 - C_{00}\right) - \frac{9m_h^2}{2}\left(\bar{c}_6 + 2\right) B_0' \right) , \\ \mathcal{F}_2(q_1^2, q_2^2) &= \frac{\lambda \bar{c}_6}{(4\pi)^2} 12\left(C_1 + C_{11} + C_{12}\right) . \end{aligned} \tag{3.5}$$

Here the arguments of the PV integrals are

$$B_0 = B_0\big(m_h^2, m_h^2, m_h^2\big) \,, \qquad C_0 = C_0\big(m_h^2, q_1^2, q_2^2, m_h^2, m_h^2, m_V^2\big) \,, \tag{3.6}$$

and analog definitions hold for the derivative B_0' of the scalar bubble integral and the tensor coefficients C_1, C_{11} and C_{12} of the triangle integral. Notice that in contrast to [31] an all-order resummation of 1-loop wave function effects is not performed in (3.5). Since already the $\mathcal{O}(\lambda^2)$ wave function corrections in the SMEFT will be incomplete due to missing 2-loop Higgs-boson selfenergy diagrams, it is questionable if such a resummation improves the precision of the calculation and we therefore do not include it our work.

4 Corrections to the Higgs partial decay widths

To determine the signal strengths in Vh and VBF Higgs production, one also has to take into account that the Higgs branching ratios are modified at the loop level by the presence of the dimension-6 operator O_6. Examples of diagrams that alter the partial widths of the Higgs to fermions, gluons and photons are displayed in Figure 2. Below we will present results for the $\mathcal{O}(\lambda)$ corrections to the partial widths of all relevant Higgs decay modes. Terms of $\mathcal{O}(\lambda^2)$ that arise from squared matrix elements with an O_6 insertion are instead dropped for consistency since such contributions receive additional but unknown corrections from the interference of tree-level SM and loop-level SMEFT amplitudes.

In the case of the decays of the Higgs to light fermion pairs $f = q, \ell$, we write

$$\Delta\Gamma(h \to f\bar{f}) = \frac{N_c^f G_F m_h m_f^2}{4\sqrt{2}\pi} \left(1 - \frac{4m_f^2}{m_h^2}\right)^{3/2} \Delta_f \,, \tag{4.1}$$

where $N_c^q = 3$, $N_c^\ell = 1$ and all quark masses m_q are understood as $\overline{\text{MS}}$ masses renormalised at the scale m_h, while m_ℓ denotes the pole mass of the corresponding lepton. The $\mathcal{O}(\lambda)$ correction to the partial decay width $\Gamma(h \to f\bar{f})$ stem from the graph displayed on the left-hand side in Figure 2. We obtain

$$\Delta_f = \frac{\lambda \bar{c}_6}{(4\pi)^2} \,\text{Re}\Big(-12 m_f^2 \,(C_0 - C_1 - C_2) - 9 m_h^2 \,(\bar{c}_6 + 2)\, B_0' \Big) \,, \tag{4.2}$$

with

$$C_0 = C_0\big(m_f^2, m_h^2, m_f^2, m_f^2, m_h^2, m_h^2\big) \,, \tag{4.3}$$

and analogue definitions for the tensor coefficients C_1 and C_2. Notice that the flavour-dependent contributions are suppressed by light-fermion masses compared to the flavour-independent contribution proportional to B_0' that arises from the wave function renormalisation of the Higgs boson. The corrections Δ_f are hence to very good approximation universal. The result (4.1) agrees numerically with [31].

The shifts in the partial width for a Higgs boson decaying into a pair of EW gauge bosons can be cast into the form [39]

$$\Delta\Gamma(h \to VV) = \frac{1}{\pi^2} \int_0^{m_h^2} \frac{dq_1^2\, m_V \Gamma_V}{(q_1^2 - m_V^2)^2 + m_V^2 \Gamma_V^2} \int_0^{(m_h - q_1)^2} \frac{dq_2^2\, m_V \Gamma_V}{(q_2^2 - m_V^2)^2 + m_V^2 \Gamma_V^2} \, I_V \,, \tag{4.4}$$

and include the contributions from both the production of one real and one virtual EW gauge boson $h \to VV^*$ or two virtual states $h \to V^*V^*$. In (4.4) the total decay width of the relevant gauge boson is denoted by Γ_V and the integrand can be written as

$$I_V = \frac{G_F m_h^3}{8\sqrt{2}\pi} \, N_V \sqrt{\alpha(q_1^2, q_2^2, m_h^2)}\, \beta(q_1^2, q_2^2, m_h^2)\, \Delta_V \,, \tag{4.5}$$

with $N_W = 1$, $N_Z = 1/2$ and

$$\alpha(x,y,z) = \Big(1 - \frac{x}{z} - \frac{y}{z}\Big)^2 - \frac{4xy}{z^2} \,, \qquad \beta(x,y,z) = \alpha(x,y,z) + \frac{12xy}{z^2} \,. \tag{4.6}$$

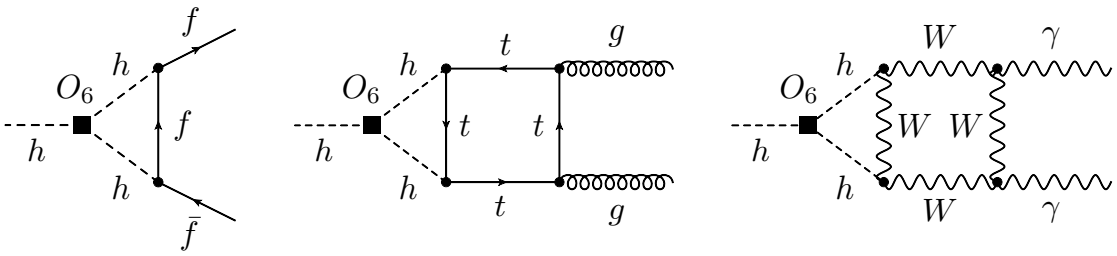

Figure 2. Feynman diagrams with an insertion of the effective operator O_6 that lead to Higgs-boson decays into fermion (left), gluon (middle) and photon (right) pairs.

The $\mathcal{O}(\lambda)$ correction to the partial decay width $\Gamma(h \to VV)$ arises from the diagrams shown in Figure 1. We find

$$\begin{aligned}\Delta_V = \frac{\lambda \bar{c}_6}{(4\pi)^2}\,\mathrm{Re}\Big[&-6B_0 - 24\left(m_V^2 C_0 - C_{00}\right) \\ &- \frac{12\alpha(q_1^2,q_2^2,m_h^2)\left(q_1^2+q_2^2-m_h^2\right)}{\beta(q_1^2,q_2^2,m_h^2)}\left(C_1+C_{11}+C_{12}\right) - 9m_h^2\left(\bar{c}_6+2\right)B_0'\Big]\,.\end{aligned} \tag{4.7}$$

Here the arguments of the PV loop integrals are defined as in (3.6). We have verified that the expression (4.4) agrees numerically with the results presented in [31].

The changes in partial decay widths of the Higgs boson to gluon and photon pairs can be written in the following way

$$\begin{aligned}\Delta\Gamma(h\to gg) &= \frac{G_F\,\alpha_s^2 m_h^3}{36\sqrt{2}\pi^3}\left|\sum_q A_q\right|^2 \Delta_g\,, \\ \Delta\Gamma(h\to \gamma\gamma) &= \frac{G_F\,\alpha^2 m_h^3}{128\sqrt{2}\pi^3}\left|\sum_f \frac{4N_c^f Q_f^2}{3}A_f - A_W\right|^2 \Delta_\gamma\,,\end{aligned} \tag{4.8}$$

where $\alpha_s = \alpha_s(m_h)$, $\alpha = 1/137.04$, while $Q_u = 2/3$, $Q_d = -1/3$ and $Q_\ell = -1$ denote the electric charges of the fermions. The leading-order (LO) form factors that encode the 1-loop corrections due to SM fermion and W-boson loops read

$$\begin{aligned}A_f &= \frac{3\tau_f}{2}\left[1+(1-\tau_f)\arctan^2\frac{1}{\sqrt{\tau_f-1}}\right]\,, \\ A_W &= 2+3\tau_W+3\tau_W(2-\tau_W)\arctan^2\frac{1}{\sqrt{\tau_W-1}}\,,\end{aligned} \tag{4.9}$$

with $\tau_X = 4m_X^2/m_h^2$ for $X = f, W$. The $\mathcal{O}(\lambda)$ correction to the partial decay width of the Higgs to gluons and photons originate from 2-loop diagrams with an insertion of O_6. Two example graphs are shown in the middle and on the right of Figure 2. The results presented

in [30, 40] lead to

$$\begin{aligned}\Delta_g &= \frac{\lambda \bar{c}_6}{(4\pi)^2}\left(8.42 - 9m_h^2\,(\bar{c}_6+2)\,B_0'\right),\\ \Delta_\gamma &= \frac{\lambda \bar{c}_6}{(4\pi)^2}\left(-3.70 - 9m_h^2\,(\bar{c}_6+2)\,B_0'\right).\end{aligned} \tag{4.10}$$

Notice that there is no need to take the real part here because the B_0' integral corresponding to a Higgs loop is real for on-shell kinematics. The expression for Δ_g agrees with the results obtained in [31].

5 Description of the Vh calculation

In order to explain how we obtain our predictions for the associated production of the Higgs boson with massive gauge bosons it is useful to first consider the $\mathcal{O}(\lambda)$ corrections to $\sigma_{Vh} = \sigma(q\bar{q} \to Vh)$ working to zeroth order in the strong coupling constant. At this order in QCD the $\mathcal{O}(\lambda)$ shift in the integrated partonic cross section can be written as

$$\Delta\sigma_{Vh} = \frac{G_F^2 m_V^4}{72\pi}\,\bar{N}_V\,\sqrt{\alpha(m_V^2,m_h^2,s)}\,\frac{\alpha(m_V^2,m_h^2,s)\,s+12m_V^2}{\left(s-m_V^2\right)^2}\,\delta_V\,, \tag{5.1}$$

with $\bar{N}_W = 1$ and $\bar{N}_Z = \left(1 - 8T_3^q Q_q s_w^2 + 8Q_q^2 s_w^4\right)/2$, where T_3^q (Q_q) denotes the third component of the weak isospin (electric charge) of the relevant quark. The function δ_V encodes the contributions from the three 1-loop diagrams in Figure 1 when one of the gauge bosons is contracted with a quark line and the other one is put on its mass shell. Explicitly we find

$$\begin{aligned}\delta_V = \frac{\lambda \bar{c}_6}{(4\pi)^2}\,\mathrm{Re}\Bigg[&-6B_0 - 24\left(m_V^2 C_0 - C_{00}\right)\\ &- \frac{12\alpha(m_V^2,m_h^2,s)\,s\left(m_V^2-m_h^2+s\right)}{\alpha(m_V^2,m_h^2,s)\,s+12m_V^2}\left(C_1+C_{11}+C_{12}\right) - 9m_h^2\,(\bar{c}_6+2)\,B_0'\Bigg],\end{aligned} \tag{5.2}$$

where the function $\alpha(x,y,z)$ has been defined in (4.6). The arguments of the scalar triangle integral are

$$C_0 = C_0\big(m_h^2, s, m_V^2, m_h^2, m_h^2, m_V^2\big)\,, \tag{5.3}$$

and all other tensor coefficients carry the same functional dependence. The B_0 integral is defined in (3.6). Our result (5.2) for δ_V can be shown to agree with the analytic expression given in the publication [28] for the case of $e^+e^- \to Zh$.

At NNLO the production cross section for $pp \to Vh$ receives corrections from two types of topologies. The first kind of graphs involves an exchange of a single off-shell vector boson in the s-channel, while the second sort of corrections arise from the coupling of the Higgs boson to a closed loop of top quarks. For on-shell bosons the former type of $\mathcal{O}(\alpha_s^2)$ corrections have been obtained in [41], while fully differential NNLO calculations of these Drell-Yan (DY) parts have been presented in [42, 43] and [44] for the Wh and Zh final

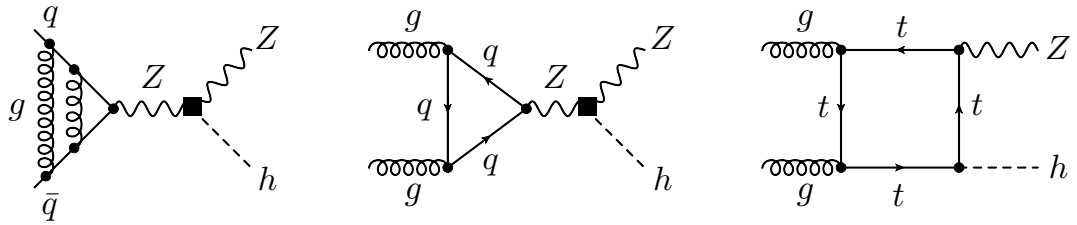

Figure 3. Examples of diagrams that contribute to $pp \to Zh$ at $\mathcal{O}(\alpha_s^2)$. As indicated by the black square the left and middle diagram receive a correction of $\mathcal{O}(\lambda)$ from δ_V, while the graph on the right-hand side does not involve a modified ZZh vertex. See text for further explanations.

state, respectively. Subsets of the diagrams where the Higgs is radiated off a top loop have been considered in [44, 45] and a calculation of all such graphs can be found in [46]. The latter results have been implemented into version 8 of `MCFM` [47].

The existing fully differential `MCFM` implementation of $pp \to Vh$ at NNLO serves as a starting point of our own computation. We have identified the routines in `MCFM` that correspond to the two different kinds of $\mathcal{O}(\alpha_s^2)$ corrections. For the case of $pp \to Zh$ representatives of the two types of contributions are displayed in Figure 3. Notice that in all diagrams where the Higgs is not radiated from a top loop the δ_V correction factorises and thus we are able to include the complete $\mathcal{O}(\lambda)$ term (5.2) on top of the NNLO corrections. In the case of the contributions with top loops however not all $\mathcal{O}(\alpha_s^2)$ corrections factorise. Non-factorisable contributions which involve a top box and a top-Higgs triangle as well as double-box contributions are in fact not known and thus cannot be included. Effects due to Higgs wave function renormalisation, on the other hand, factorise and we take them into account in our computations. As a result, our numerical predictions for the differential $pp \to Vh$ cross sections are NNLO accurate only for what concerns the $\mathcal{O}(\lambda)$ terms associated to δ_V, while we are missing $\mathcal{O}(\alpha_s^2)$ contributions proportional to $\lambda\bar{c}_6$ that stem from top loops.

6 Description of the VBF Higgs calculation

To obtain predictions for VBF Higgs production we employ the structure-function approach [48]. In this formalism the VBF Higgs process can be described to high accuracy as a double deep-inelastic scattering process (DIS), where two virtual EW gauge bosons emitted from the hadronic initial states fuse into a Higgs boson. Neglecting small QCD-interference effects between the two inclusive final states, the differential VBF Higgs cross section is in our case given by a product of two 3-point vertices $\Gamma_V^{\mu\nu}(Q_1, Q_2)$ and two DIS hadronic tensors $W_V^{\mu\nu}(x_i, Q_i^2)$:

$$\begin{aligned} d\sigma_{\rm VBF} = {} & \frac{G_F^2 m_V^4}{s}\, \Delta_V^2(Q_1^2)\Delta_V^2(Q_2^2) \\ & \times W_{\mu\nu}^V(x_1, Q_1^2)\, \Gamma_V^{\mu\rho}(Q_1, Q_2)\, \big(\Gamma_V^{\nu\sigma}(Q_1, Q_2)\big)^*\, W_{\rho\sigma}^V(x_2, Q_2^2)\, d\Omega\,. \end{aligned} \tag{6.1}$$

Here $\Delta_V(Q_i^2) = 1/(Q_i^2 + m_V^2)$, $Q_i^2 = -q_i^2$ and $x_i = Q_i^2/(2P_i \cdot q_i)$ are the usual DIS variables with P_i^μ the 4-momentum of proton $i = 1, 2$ and $d\Omega$ denotes the 3-particle VBF phase space. The hadronic tensor can be expressed as

$$\begin{aligned} W_V^{\mu\nu}(x_i, Q_i^2) = &\left(-\eta^{\mu\nu} - \frac{q_i^\mu q_i^\nu}{Q_i^2}\right) F_1^V(x_i, Q_i^2) + \frac{\hat{P}_i^\mu \hat{P}_i^\nu}{P_{ii}} F_2^V(x_i, Q_i^2) \\ &+ i\epsilon^{\mu\nu\rho\sigma} \frac{P_{i\rho} q_{i\sigma}}{2P_{ii}} F_3^V(x_i, Q_i^2)\,, \end{aligned} \tag{6.2}$$

where $\epsilon^{\mu\nu\rho\sigma}$ is the fully anti-symmetric Levi-Civita tensor and we have introduced

$$P_i \cdot q_j = P_{ij}\,, \qquad \hat{P}_i^\mu = P_i^\mu + \frac{P_{ii}}{Q_i^2} q_i^\mu\,. \tag{6.3}$$

The standard DIS structure functions are denoted by $F_m^V(x_i, Q_i^2)$ with $m = 1, 2, 3$.

Using the decomposition (6.2) the squared hadronic tensor in (6.1) can be written in terms of the DIS structure functions as

$$\begin{aligned} &W_{\mu\nu}^V(x_1, Q_1^2)\, \Gamma_V^{\mu\rho}(Q_1, Q_2) \left(\Gamma_V^{\nu\sigma}(Q_1, Q_2)\right)^* W_{\rho\sigma}^V(x_2, Q_2^2) = \\ &\qquad\qquad 4\sqrt{2} G_F m_V^4 \sum_{m,n}^{3} w_{mn} F_m^V(x_1, Q_1^2) F_n^V(x_2, Q_2^2)\,. \end{aligned} \tag{6.4}$$

Defining the short-hand notations[2]

$$q_1 \cdot q_2 = q_{12}\,, \quad P_1 \cdot P_2 = p_{12}\,, \quad \mathcal{C}_1 = 1 + 2\mathcal{F}_1(Q_1^2, Q_2^2)\,, \quad \mathcal{C}_2 = 2\mathcal{F}_2(Q_1^2, Q_2^2)\,, \tag{6.5}$$

the non-vanishing coefficients w_{mn} included in our analysis read

$$\begin{aligned} w_{11} &= (2\mathcal{C}_1 - q_{12}\mathcal{C}_2) + (\mathcal{C}_1 + q_{12}\mathcal{C}_2) \frac{q_{12}^2}{Q_1^2 Q_2^2}\,, \\ w_{12} &= -\mathcal{C}_1 \frac{P_{22}}{Q_2^2} - (\mathcal{C}_1 + q_{12}\mathcal{C}_2) \left(\frac{P_{21}^2}{P_{22} Q_1^2} + \frac{2P_{21}\, q_{12}}{Q_1^2 Q_2^2} + \frac{P_{22}\, q_{12}^2}{Q_1^2 Q_2^4}\right)\,, \\ w_{21} &= -\mathcal{C}_1 \frac{P_{11}}{Q_1^2} - (\mathcal{C}_1 + q_{12}\mathcal{C}_2) \left(\frac{P_{12}^2}{P_{11} Q_2^2} + \frac{2P_{12}\, q_{12}}{Q_1^2 Q_2^2} + \frac{P_{11}\, q_{12}^2}{Q_1^4 Q_2^2}\right)\,, \\ w_{22} &= \frac{1}{P_{11} P_{22} Q_1^4 Q_2^4} \Big[\mathcal{C}_1 \left(p_{12} Q_1^2 Q_2^2 + P_{11} P_{21} Q_2^2 + P_{12} P_{22} Q_1^2 + P_{11} P_{22}\, q_{12}\right)^2 \\ &\quad + \mathcal{C}_2 \left(P_{12} Q_1^2 + P_{11}\, q_{12}\right) \left(P_{21} Q_2^2 + P_{22}\, q_{12}\right) \\ &\quad \times \left(p_{12} Q_1^2 Q_2^2 + P_{11} P_{21} Q_2^2 + P_{12} P_{22} Q_1^2 + P_{11} P_{22}\, q_{12}\right) \Big]\,, \\ w_{33} &= \frac{1}{4 P_{11} P_{22}} \Big[2\mathcal{C}_1 \left(p_{12}\, q_{12} - P_{12} P_{21}\right) \\ &\quad - \mathcal{C}_2 \left\{ P_{12} P_{22} Q_1^2 + \left(p_{12} Q_1^2 + P_{11} P_{21}\right) Q_2^2 + \left(P_{11} P_{22} + P_{12} P_{21}\right) q_{12} - p_{12}\, q_{12}^2 \right\} \Big]\,. \end{aligned} \tag{6.6}$$

[2]For VBF kinematics the form factor $\mathcal{F}_{1,2}(Q_1^2, Q_2^2)$ are real and in consequence there is no need to take the real part in the last two definitions in (6.5).

Notice that in the above expressions for the coefficients w_{mn} we have neglected terms quadratic in the form factors $\mathcal{F}_{1,2}(Q_1^2, Q_2^2)$. Such contributions are suppressed relative to the linear terms in (6.6) by a factor of $\lambda\bar{c}_6/(4\pi)^2$ and thus formally of 2-loop order in the SMEFT. Since the 2-loop SMEFT contributions to the $\mathcal{O}(\lambda^2)$ corrections remain unknown including terms quadratic in (3.5) would thus not improve the accuracy of the calculation.

With all the non-vanishing coefficients w_{mn} at hand it is now rather straightforward to calculate NNLO QCD corrections to the inclusive [49, 50] and exclusive [51] VBF Higgs cross section.[3] Our computations rely on the techniques and the Monte Carlo (MC) codes developed in the latter work. In the inclusive part of the calculation, we employ the phase space from the $h + 2\,\text{jets}$ VBF calculation implemented in `POWHEG` [53], while the matrix element is evaluated with structure functions based on parametrised versions [54, 55] of the NNLO DIS coefficient functions [56–58] integrated with `HOPPET` [59]. The exclusive calculation relies also on the NLO part of the `POWHEG` $h + 3\,\text{jets}$ VBF code [60], which implements the results of [61]. To take into account contributions from the second Lorentz structure in (3.1) the SM implementation [60] had to be extended. This extension required, in particular, new tree-level $h + 4\,\text{jets}$ matrix elements, which were generated with `MadGraph5_aMCNLO` [62]. The numerical evaluation of 1-loop Feynman integrals is performed by `QCDLoop` [63, 64] after reducing the tensor coefficients appearing in (3.3) to basic PV scalar integrals. Further technical details on the implementation of the NNLO VBF Higgs cross section computations are given in [51].

7 Numerical results

In this section we study the numerical impact of the $\mathcal{O}(\lambda)$ corrections that we have derived earlier in Sections 3 and 4. We first present results for the modifications of the Higgs production cross sections σ_I in the vector boson mediated channels $I = Wh, Zh, \text{VBF}$. Then we study the corrections to the partial Higgs decay widths $\Gamma^F = \Gamma(h \to F)$ and branching ratios $\text{Br}^F = \text{Br}(h \to F)$. This discussion is followed by an analysis of the shape changes in the Vh and VBF Higgs distributions due to the $\mathcal{O}(\lambda)$ corrections. We finally derive the constraints on the Wilson coefficient $\bar{c}_6$ that arise from LHC Run I and II data, and explore the prospects of the HL-LHC in improving the current bounds. Both the limits from double-Higgs production as well as Vh and VBF Higgs production are considered.

7.1 Modifications of the Higgs production cross sections

We begin our discussion by considering the modifications of the inclusive vector boson mediated Higgs production sections σ_I that result from the presence of the $\mathcal{O}(\lambda)$ corrections. The corresponding predictions are shown in the two panels of Figure 4 as a function of $\bar{c}_6$. In the left plot we display the total cross sections for pp collisions at $\sqrt{s} = 8\,\text{TeV}$ (dashed

[3] Very recently the next-to-next-to-next-to-leading order (N^3LO) QCD corrections to the inclusive VBF Higgs cross section have been calculated in the structure-function approach [52]. We do not include N^3LO effects in our analysis since they amount to $\mathcal{O}(1‰)$ shifts, which is well within the NNLO scale uncertainties.

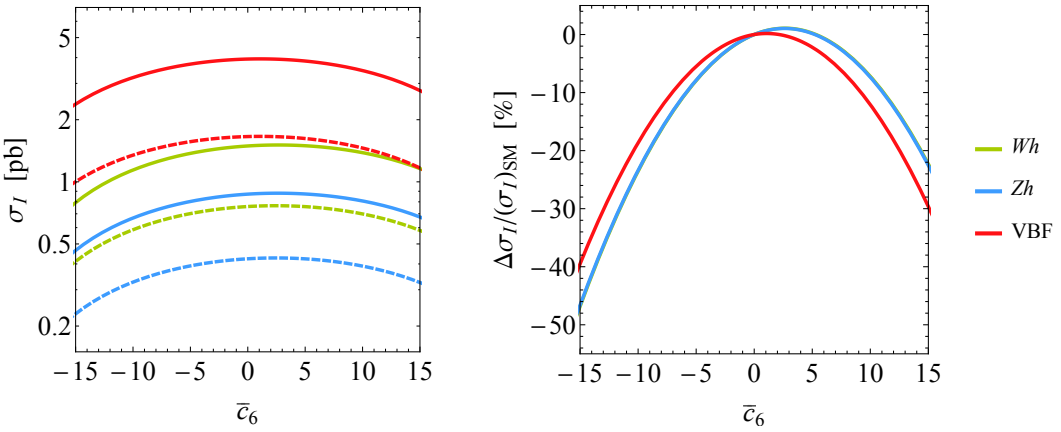

Figure 4. Left: Predictions for the inclusive Wh, Zh and VBF Higgs production sections σ_I as a function of $\bar{c}_6$. The dashed and solid curves correspond to $\sqrt{s} = 8\,\text{TeV}$ and $\sqrt{s} = 13\,\text{TeV}$, respectively. Right: Relative modifications of σ_I as a function of the Wilson coefficient of O_6. Only results for $\sqrt{s} = 13\,\text{TeV}$ are shown.

curves) and $\sqrt{s} = 13\,\text{TeV}$ (solid curves). In the former case, we find

$$\begin{aligned}
\sigma_{Wh}^{8\,\text{TeV}} &= (\sigma_{Wh}^{8\,\text{TeV}})_{\text{SM}} \left(1 + 7.4 \cdot 10^{-3}\, \bar{c}_6 - 1.5 \cdot 10^{-3}\, \bar{c}_6^2\right) , \\
\sigma_{Zh}^{8\,\text{TeV}} &= (\sigma_{Zh}^{8\,\text{TeV}})_{\text{SM}} \left(1 + 7.5 \cdot 10^{-3}\, \bar{c}_6 - 1.5 \cdot 10^{-3}\, \bar{c}_6^2\right) , \\
\sigma_{\text{VBF}}^{8\,\text{TeV}} &= (\sigma_{\text{VBF}}^{8\,\text{TeV}})_{\text{SM}} \left(1 + 3.3 \cdot 10^{-3}\, \bar{c}_6 - 1.5 \cdot 10^{-3}\, \bar{c}_6^2\right) ,
\end{aligned} \tag{7.1}$$

where the prediction for the Wh cross section includes both the $pp \to W^+h$ and the $pp \to W^-h$ channel. The SM predictions that enter the above formulas read $(\sigma_{Wh}^{8\,\text{TeV}})_{\text{SM}} = (0.76 \pm 0.02)\,\text{pb}$, $(\sigma_{Zh}^{8\,\text{TeV}})_{\text{SM}} = (0.42 \pm 0.01)\,\text{pb}$ and $(\sigma_{\text{VBF}}^{8\,\text{TeV}})_{\text{SM}} = (1.66 \pm 0.04)\,\text{pb}$. In the latter case, we instead obtain

$$\begin{aligned}
\sigma_{Wh}^{13\,\text{TeV}} &= (\sigma_{Wh}^{13\,\text{TeV}})_{\text{SM}} \left(1 + 8.2 \cdot 10^{-3}\, \bar{c}_6 - 1.5 \cdot 10^{-3}\, \bar{c}_6^2\right) , \\
\sigma_{Zh}^{13\,\text{TeV}} &= (\sigma_{Zh}^{13\,\text{TeV}})_{\text{SM}} \left(1 + 8.0 \cdot 10^{-3}\, \bar{c}_6 - 1.5 \cdot 10^{-3}\, \bar{c}_6^2\right) , \\
\sigma_{\text{VBF}}^{13\,\text{TeV}} &= (\sigma_{\text{VBF}}^{13\,\text{TeV}})_{\text{SM}} \left(1 + 3.3 \cdot 10^{-3}\, \bar{c}_6 - 1.5 \cdot 10^{-3}\, \bar{c}_6^2\right) ,
\end{aligned} \tag{7.2}$$

and the relevant SM cross sections are $(\sigma_{Wh}^{13\,\text{TeV}})_{\text{SM}} = (1.49 \pm 0.03)\,\text{pb}$, $(\sigma_{Zh}^{13\,\text{TeV}})_{\text{SM}} = (0.87 \pm 0.03)\,\text{pb}$ and $(\sigma_{\text{VBF}}^{13\,\text{TeV}})_{\text{SM}} = (3.94 \pm 0.08)\,\text{pb}$. Our results have been obtained with the implementations of the Vh and VBF Higgs calculations described in Sections 5 and 6. They correspond to `PDF4LHC15_nnlo_mc` parton distribution functions (PDFs) [65] and the quoted uncertainties include both scale, PDF and α_s errors. In the case of Vh (VBF Higgs) production our default scale choice is $\mu_0 = m_V + m_h$ ($\mu_0 = m_h$). The perturbative uncertainties are estimated in both cases by identifying the renormalisation and factorisation scales μ_R and μ_F with μ_0 and varying μ_0 by a factor of two around the default scale.

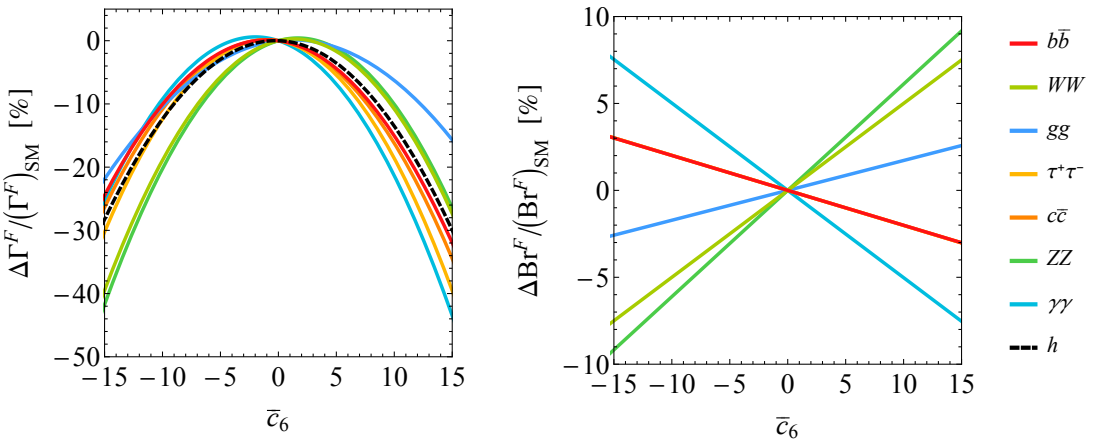

Figure 5. Shifts in the partial decay widths (left panel) and the branching ratios (right panel) of the Higgs boson as a function of the Wilson coefficient $\bar{c}_6$. The coloured curves indicate the individual decay channels, while the black dashed curve corresponds to the total Higgs decay width.

The above formulas can be compared to the next-to-leading order (NLO) results for the Vh and VBF Higgs production cross sections presented in [31]. Concerning σ_{Wh} and $\sigma_{\rm VBF}$, we find that the inclusion of $\mathcal{O}(\alpha_s^2)$ corrections essentially does not change the functional dependence on $\bar{c}_6$ compared to NLO. In the case of σ_{Zh}, NNLO effects have instead an impact since they shift the term linear in $\bar{c}_6$ by around -20% (-10%) compared to the 8 TeV (13 TeV) NLO prediction. The observed shifts originate from the negative $\mathcal{O}(\alpha_s^2)$ contributions due to heavy-quark boxes of the type $gg \to Zh$. Given that the corresponding non-universal $\mathcal{O}(\lambda)$ corrections are not included in our calculation (see the discussion in Section 5) it remains unclear whether the inclusion of NNLO effects improves the precision of our $pp \to Zh$ predictions. We add that we have verified that at NLO our numerical results for Vh and VBF Higgs production all agree with the predictions given in [31].

Looking at the results (7.1) and (7.2) one observes that the linear dependence on the Wilson coefficient $\bar{c}_6$ of the Vh and VBF Higgs cross sections is different. This feature is expected because the terms linear in $\bar{c}_6$ originate from both tree-level counterterm graphs involving a Higgs wave function renormalisation as well as the interference of tree-level with 1-loop amplitudes. While the Higgs wave function renormalisation constant depends only on m_h, the interference contributions have a non-trivial dependence on the external 4-momenta. As a result the $\mathcal{O}(\bar{c}_6)$ terms are process and kinematics dependent. To better illustrate the numerical impact of the $\mathcal{O}(\lambda)$ corrections, we plot $\Delta\sigma_I/(\Delta\sigma_I)_{\rm SM}$ as a function of $\bar{c}_6$ in the right panel of Figure 4 employing $\sqrt{s} = 13\,\text{TeV}$. We see that for $\bar{c}_6 \simeq -15$ the Vh and VBF Higgs cross sections are shifted by about -50% and -40%, while for $\bar{c}_6 \simeq 15$ the corresponding shifts are around -25% and -30%. Given that the functional dependencies of (7.1) and (7.2) are approximately the same, effects of similar size are obtained at $\sqrt{s} = 8\,\text{TeV}$. The corresponding predictions are not shown in the latter figure.

7.2 Modifications of the Higgs decays

We now turn our attention to the partial decay widths and branching ratios of the Higgs. In Figure 5 we illustrate the numerical impact of the $\mathcal{O}(\lambda)$ corrections on these observables. As input parameters we have used $\alpha_s(m_h) = 0.1127$, $m_t = 173.2\,\text{GeV}$, $m_b(m_h) = 2.81\,\text{GeV}$, $m_c(m_h) = 0.65\,\text{GeV}$, $m_\tau = 1.777\,\text{GeV}$, $m_W = 80.37\,\text{GeV}$, $m_Z = 91.15\,\text{GeV}$, $\Gamma_W = 2.0886\,\text{GeV}$ and $\Gamma_Z = 2.4958\,\text{GeV}$. The quoted values for the bottom and charm quark $\overline{\text{MS}}$ masses have been obtained by employing 2-loop running. The SM predictions for the total decay width of the Higgs and its branching ratios are taken from [66]. In the case of the partial decay widths (left panel), one observes that the relative corrections to Γ^F all have a very similar $\bar{c}_6$ dependence and are essentially always negative. These features are related to the fact that for $|\bar{c}_6| \gtrsim 1$ the partial decay widths are dominated by the universal corrections arising from the Higgs wave function renormalisation which is quadratic in $\bar{c}_6$ and carries a minus sign. Numerically, we find that the relative shifts in Γ^F can reach up to around -40% (-45%) for $\bar{c}_6 \simeq -15$ ($\bar{c}_6 \simeq 15$). The corrections to the total decay width Γ_h are only about -30%. In the case of the shifts in the Higgs branching ratios (right panel), one observes instead that the modifications in all channels do not exceed $\pm 10\%$ in the same $\bar{c}_6$ range. The impact of $\mathcal{O}(\lambda)$ corrections is thus generically smaller in the branching ratios than in the partial decay widths, since in the former quantities the universal Higgs wave function corrections and thus the quadratic dependence on $\bar{c}_6$ cancels.

7.3 Modifications of the Vh and VBF Higgs distributions

Since the vertex corrections (3.1) depend in a non-trivial way on the external 4-momenta, the $\mathcal{O}(\lambda)$ corrections not only change the overall size of the cross sections in Vh and VBF Higgs production but also modify the shape of the corresponding kinematic distributions. In this subsection we present results for the spectra that are most sensitive to modifications in the trilinear Higgs coupling. All results shown below correspond to $\sqrt{s} = 13\,\text{TeV}$, `PDF4LHC15_nnlo_mc` PDFs and the default scale choices introduced in Section 7.1. Off-shell effects in Higgs-boson production are taken into account by modelling the width of the Higgs with a Breit-Wigner line shape.

We begin our discussion with $pp \to Wh$. In Figure 6 the distributions of the Higgs-boson transverse momentum ($p_{T,h}$) and the invariant mass of the Wh system (m_{Wh}) are shown. The black curves in the panels represent the SM predictions, while the blue and red curves correspond to a new-physics scenario with $\bar{c}_6 = -10$ and $\bar{c}_6 = 10$, respectively. All results have been obtained at NNLO with the MC code described in Section 5. One sees that the shape of the displayed distributions provide sensitivity to the sign of $\bar{c}_6$. In the case of $\bar{c}_6 = -10$ the $p_{T,h}$ (m_{Wh}) spectrum increases relative to the SM distribution as a function of $p_{T,h}$ (m_{Wh}), approaching a constant value in the limit of large $p_{T,h}$ (m_{Wh}). For $\bar{c}_6 = 10$ the ratio R instead decreases with $p_{T,h}$ (m_{Wh}) becoming again flat for $p_{T,h} \to \infty$ ($m_{Wh} \to \infty$). The behaviour of the distribution for large $p_{T,h}$ and m_{Wh} can be understood from the $\sqrt{s} \to \infty$ limit of (5.2). In this limit only the Higgs wave function renormalisation

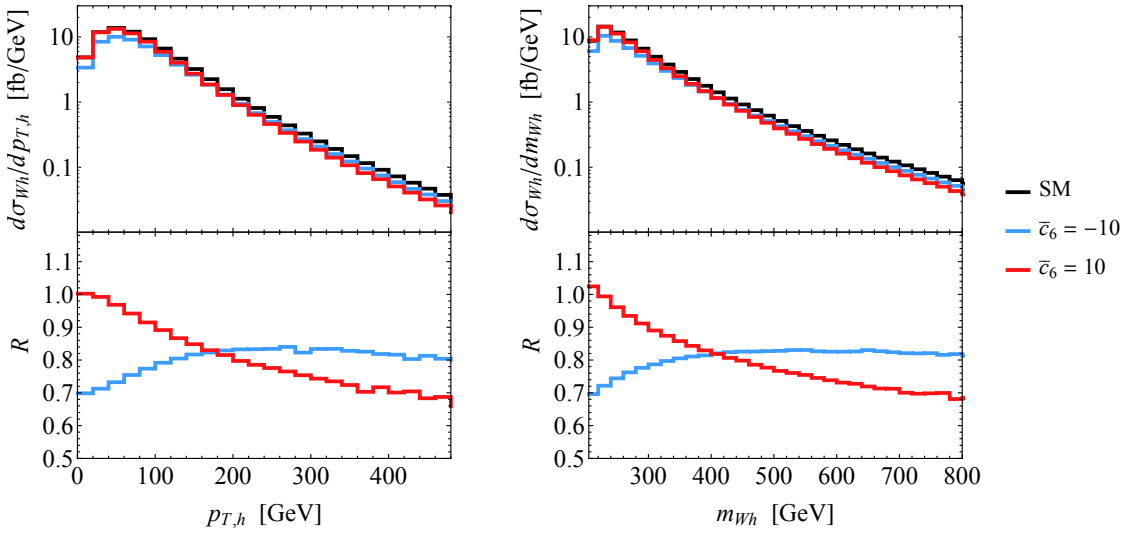

Figure 6. Comparison of the $p_{T,h}$ (left) and m_{Wh} (right) spectrum in Wh production. The upper panels show the SM predictions (black) as well as the cases $\bar{c}_6 = -10$ (blue) and $\bar{c}_6 = 10$ (red). The ratios between the case $\bar{c}_6 = -10$ and the SM (blue) and the case $\bar{c}_6 = 10$ and the SM (red) are displayed in the lower panels. All results correspond to pp collisions at $\sqrt{s} = 13\,\text{TeV}$.

contributes and the vertex correction δ_V takes the simple form

$$\lim_{\sqrt{s}\to\infty} \delta_V = \frac{\lambda \bar{c}_6}{(4\pi)^2} \left(-9 m_h^2 \left(\bar{c}_6 + 2\right) B_0'\right) = -1.5 \cdot 10^{-3}\, \bar{c}_6 \left(\bar{c}_6 + 2\right) . \tag{7.3}$$

It follows that for large transverse momenta (invariant masses) the deviation from 1 of the ratio R of the $p_{T,h}$ (m_{Wh}) spectrum for $\bar{c}_6 \neq 0$ and $\bar{c}_6 = 0$, i.e. the SM distribution, is approximately given by (7.3). New-physics scenarios with $\bar{c}_6 < 0$ will hence lead to harder $p_{T,h}$ and m_{Wh} tails than cases with $\bar{c}_6 > 0$, while they predict softer spectra at low $p_{T,h}$ and m_{Wh}. These features are clearly visible in Figure 6 and are also present in other kinematical observables such as the transverse momentum $p_{T,W}$ of the W boson. The shapes of all rapidity distributions in $pp \to Wh$ production are in contrast largely insensitive to the sign of $\bar{c}_6$. Notice that our general arguments also apply to the case of $pp \to Zh$, and as a result the distributions in the Zh channel resemble those found in Wh production. We therefore do not show predictions for the various Zh spectra.

In Figure 7 we present our results for two kinematic distributions in VBF Higgs production, namely the Higgs transverse momentum $p_{T,h}$ and the transverse momentum of the third jet p_{T,j_3}. The spectra shown are obtained with the fully-differential NNLO VBF code described in Section 6 and correspond to the following selection cuts. Events should have at least two jets with $p_{T,j} > 25\,\text{GeV}$, the two jets with highest $p_{T,j}$ are required to have an absolute rapidity of $|y_j| < 4.5$, be separated by $\Delta y_{j_1,j_2} > 5$ in rapidity, have an invariant mass $m_{j_1,j_2} > 600\,\text{GeV}$ and be in opposite hemispheres (i.e. $y_{j_1} y_{j_2} < 0$). In our analysis jets

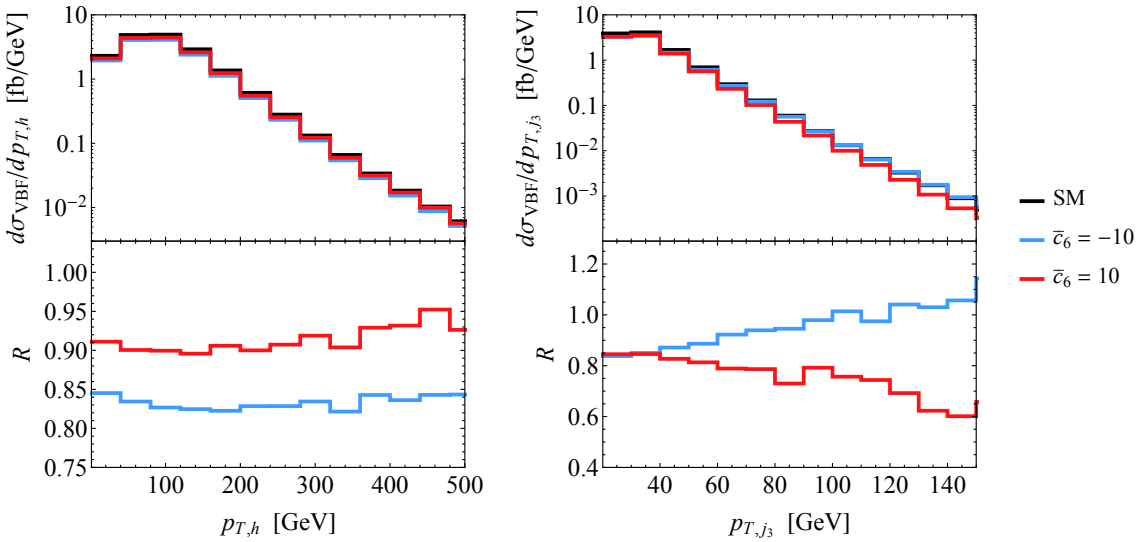

Figure 7. Comparison of the $p_{T,h}$ (left) and p_{T,j_3} (right) spectrum in VBF Higgs production. The style and colour coding of the curves follows the one of Figure 6.

are defined using the anti-k_t algorithm [67], as implemented in `FastJet` [68], with radius parameter of 0.4. As before we present results for the benchmark scenarios $\bar{c}_6 = -10$ (blue curves) and $\bar{c}_6 = 10$ (red curves) and compare them to the SM predictions (black curves). From the left panel in the figure we see that the shape of the $p_{T,h}$ distribution in VBF Higgs production is modified only mildly by the presence of new physics in the h^3 coupling, and in consequence the ratio to the SM is almost constant in $p_{T,h}$. This feature can be explained by realising that even for large $p_{T,h}$ one of the squared momenta Q_1^2 or Q_2^2 that enters the form factors $\mathcal{F}_{1,2}(Q_1^2, Q_2^2)$ (see (6.5)) can be small. As a result for fixed $p_{T,h}$ a range of $Q_{1,2}^2$ values is probed and the constant ratio to the SM reflects this averaging. Similar averagings also take place for instance for the transverse momentum of the first and second hardest jet, and hence the ratios R corresponding to p_{T,j_1} and p_{T,j_2} turn out to be almost flat as well. On the contrary, when the third jet is hard both $Q_{1,2}^2$ tend to be hard. An increase in magnitude of both $Q_{1,2}^2$ gives rise to an approximately linear modification of the form factors $\mathcal{F}_{1,2}(Q_1^2, Q_2^2)$. This results in a linear shape in the ratio to the SM, as can be seen from the right panel in Figure 7. Still the effects are relatively small for the p_{T,j_3} values accessible at the LHC, which will limit the discriminating power of shape analyses in the VBF Higgs production channel.

7.4 Constraints on $\bar{c}_6$ from double-Higgs production

In the next subsection will derive the existing and possible future limits on the modifications of the trilinear Higgs-boson coupling that arise from Vh and VBF Higgs production. All the numbers that we will present should be compared to the bounds that one can obtain by

studying $pp \to hh$ production at the LHC. For definiteness we will assume throughout our numerical analysis that the modifications of the Wilson coefficient of the operator O_6 furnish the dominant contribution to the observable under consideration, and consequently neglect effects associated to other dimension-6 operators such as for instance O_H — see (2.2).

The ATLAS collaboration has recently performed a search for Higgs-boson pair production in the $2b2\bar{b}$ final state using $13.3\,\text{fb}^{-1}$ of $\sqrt{s} = 13\,\text{TeV}$ data [69]. From this measurement the cross section times branching ratio for non-resonant SM Higgs-boson pair production is constrained to be less than 330 fb, which is approximately 29 times above the SM expectation of $(\sigma^{13\,\text{TeV}}_{2b2\bar{b}})_{\text{SM}} = (11.3^{+0.9}_{-1.0})\,\text{pb}$. By employing `HPAIR` [70, 71], we obtain

$$\sigma^{13\,\text{TeV}}_{2b2\bar{b}} = (\sigma^{13\,\text{TeV}}_{2b2\bar{b}})_{\text{SM}} \; \left(1 - 0.82\,\bar{c}_6 + 0.29\,\bar{c}_6^2\right) \text{pb}\,. \tag{7.4}$$

From this formula we find that the ATLAS limit on the $pp \to 2h \to 2b2\bar{b}$ production cross section translates into the following 95% confidence level (CL) bound

$$\bar{c}_6 \in [-9.5, 12.3]\,, \tag{7.5}$$

if theoretical uncertainties are taken into account. Note that (7.5) improves on the bound of $\bar{c}_6 \in [-15.5, 18.1]$ that has been derived in [30] from the ATLAS Run I searches for $pp \to hh$ [72–74] by around 35%. It follows that the combination λc_3 introduced in (2.3) can at present still deviate from the SM trilinear Higgs coupling λ by a factor of roughly 11.

The small rate, the mild dependence of the cross section on λ and the difficulty of selecting signal from backgrounds make determinations of the trilinear Higgs coupling in $pp \to 2h$ production challenging even at the HL-HLC. For instance the ATLAS study of the $2b2\gamma$ final state [23] foresees a 95% CL limit of

$$\bar{c}_6 \in [-2.3, 7.7]\,, \tag{7.6}$$

assuming $3\,\text{ab}^{-1}$ of integrated luminosity. Multivariate analyses (MVAs) and/or combinations of $2b2\gamma$ with other decay channels such as $2\tau 2b$ [26] or $2b2\bar{b}$ may allow to improve (7.6), by how much precisely is however unclear at present.

7.5 Constraints on $\bar{c}_6$ from Vh and VBF Higgs production

Since only the product of the production cross sections σ_I and branching ratios Br^F of the Higgs boson can be extracted experimentally, it has become customary to define the signal strengths

$$\mu_I^F = \frac{\sigma_I}{(\sigma_I)_{\text{SM}}} \frac{\text{Br}^F}{(\text{Br}^F)_{\text{SM}}}\,, \tag{7.7}$$

which characterise the Higgs boson yields in a specific production and decay channel relative to the SM expectations. The formalisms of signal strengths can then be used to test the compatibility of the LHC measurements with the SM and to interpret the Higgs data in the context of BSM searches.

To obtain the current constraints on $\bar{c}_6$ we use the LHC Run I combination of the ATLAS and CMS measurements of the Higgs boson production and decay rates [1]. In the

case of the vector boson mediated production processes the relevant μ_I^F parameters read

$$\begin{aligned} \mu_V^{b\bar{b}} &= 0.65^{+0.30}_{-0.29}\,, \qquad \mu_V^{WW} = 1.38^{+0.41}_{-0.37}\,, \\ \mu_V^{\tau^+\tau^-} &= 1.12^{+0.37}_{-0.35}\,, \qquad \mu_V^{ZZ} = 0.48^{+1.37}_{-0.91}\,, \qquad \mu_V^{\gamma\gamma} = 1.05^{+0.44}_{-0.41}\,, \end{aligned} \tag{7.8}$$

where the subscript V indicates that the above numbers correspond to a combination of the Vh and VBF channels. These numbers have been obtained from a 10-parameter fit to each of the five decay channels and can be found in the upper part of Table 13 of [1]. The quoted uncertainties take into account the experimental uncertainty in the measurement of μ_I^F as well as the SM theory error associated to each particular channel. In the following we will employ this framework to set limits on the Wilson coefficient $\bar{c}_6$.

Using our predictions for σ_I and Br^F presented in Sections 7.1 and 7.2 we then can calculate the signal strengths μ_I^F and compare them to experiment. Including the errors quoted in (7.8) but neglecting theoretical uncertainties associated to missing λ terms, we obtain the limit

$$\bar{c}_6 \in [-13.6, 16.9]\,, \quad \text{(LHC Run I)}\,, \tag{7.9}$$

by performing a χ^2 fit with $\Delta\chi^2 = 3.84$ which corresponds to a 95% CL for a Gaussian distribution. This constraint is somewhat weaker than both the bound (7.5) as well as the limit of $\bar{c}_6 \in [-11.9, 10.3]$ that follows from a combination of the $gg \to h$ and $h \to \gamma\gamma$ channels [30, 40]. Notice that our bound (7.9) compares well with the current limits on the modifications of the trilinear Higgs coupling reported in [31].

The experimental prospects for measuring the Higgs boson signal strengths (7.7) in the vector boson mediated production modes at future LHC runs has been studied by both the ATLAS and CMS collaborations [75–80]. To estimate the sensitivity on $\bar{c}_6$ that can be reached at the HL-LHC with $3\,\mathrm{ab}^{-1}$ of data, we study two benchmark scenarios based on the results reported in the fourth and fifth column of Table 1 of [77].[4] Our first scenario includes the current theory uncertainties and reads

$$\begin{aligned} \Delta\mu_{Wh}^{b\bar{b}} &= \pm 37\%\,, \quad \Delta\mu_{Wh}^{\gamma\gamma} = \pm 19\%\,, \\ \Delta\mu_{Zh}^{b\bar{b}} &= \pm 14\%\,, \quad \Delta\mu_{Zh}^{\gamma\gamma} = \pm 28\%\,, \quad \Delta\mu_{Vh}^{ZZ} = \pm 13\%\,, \\ \Delta\mu_{\mathrm{VBF}}^{WW} &= \pm 15\%\,, \quad \Delta\mu_{\mathrm{VBF}}^{\tau^+\tau^-} = \pm 19\%\,, \quad \Delta\mu_{\mathrm{VBF}}^{ZZ} = \pm 21\%\,, \quad \Delta\mu_{\mathrm{VBF}}^{\gamma\gamma} = \pm 22\%\,, \end{aligned} \tag{7.10}$$

whereas in the second benchmark scenario theoretical errors are not taken into account. The corresponding relative uncertainties are

$$\begin{aligned} \Delta\mu_{Wh}^{b\bar{b}} &= \pm 36\%\,, \quad \Delta\mu_{Wh}^{\gamma\gamma} = \pm 17\%\,, \\ \Delta\mu_{Zh}^{b\bar{b}} &= \pm 13\%\,, \quad \Delta\mu_{Zh}^{\gamma\gamma} = \pm 27\%\,, \quad \Delta\mu_{Vh}^{ZZ} = \pm 12\%\,, \\ \Delta\mu_{\mathrm{VBF}}^{WW} &= \pm 9\%\,, \quad \Delta\mu_{\mathrm{VBF}}^{\tau^+\tau^-} = \pm 15\%\,, \quad \Delta\mu_{\mathrm{VBF}}^{ZZ} = \pm 16\%\,, \quad \Delta\mu_{\mathrm{VBF}}^{\gamma\gamma} = \pm 15\%\,. \end{aligned} \tag{7.11}$$

[4] The inclusion of further channels such as for instance $pp \to Vh\,(h \to \tau^+\tau^-)$ [81] or technical developments like extended jet tracking [82] are expected to result in an improved precision on the signals strengths μ_I^F. In order to obtain a conservative future limit on the Wilson coefficient $\bar{c}_6$ we do not consider such improvements.

Notice that compared to the CMS projections [79] our HL-LHC benchmark uncertainties $\Delta\mu_I^F$ are comparable but in all cases slightly larger, irrespectively of whether or not theory errors are included in the final numbers.

Assuming that the central values of the future HL-LHC measurements coincide in every channel with the predictions of the SM, we obtain the following 95% CL limit on the Wilson coefficient of O_6 from our χ^2 fit

$$\bar{c}_6 \in [-7.0, 10.9]\,, \quad \text{(HL-LHC, all uncertainties)}\,, \tag{7.12}$$

when all uncertainties are included. If theoretical errors are neglected, we instead find

$$\bar{c}_6 \in [-6.2, 9.6]\,, \quad \text{(HL-LHC, no theory uncertainty)}\,. \tag{7.13}$$

These limits improve on the current constraint (7.9) by a factor of around 1.7 to 2, depending on how theory errors are treated. They should be compared to the determination (7.6) of $\bar{c}_6$ in double-Higgs production. We see that with the full HL-LHC data set the indirect determination of $\bar{c}_6$ through measurements of $pp \to Vh$ and $pp \to jjh$ should allow to test shifts in the trilinear Higgs coupling that are at the same level than the more direct extraction via $pp \to hh$. A comparison of (7.12) and (7.13) also shows that theoretical uncertainties are not a limiting factor for the extraction of $\bar{c}_6$ through measurements of Vh and VBF Higgs production.

We finally add that future LHC combinations of the cross section measurements of $pp \to Vh$ and $pp \to jjh$ with those of $gg \to h$ [30, 31] and $pp \to t\bar{t}h$ [31] are expected to further strengthen the indirect constraints on the Wilson coefficient of the operator O_6. Differential information from single Higgs production and/or decays may also be used to improve the sensitivity on $\bar{c}_6$. Making the latter statement more precise would require a MVA of the prospects to measure Vh and VBF Higgs distributions in the HL-LHC environment building on the results presented in Section 7.3. Such a study is however beyond the scope of this article.

8 Conclusions

The main goal of this work was to constrain possible deviations in the h^3 coupling using measurements of Vh and VBF Higgs production in pp collisions. In order to keep the entire discussion model independent, we have adopted the SMEFT framework, in which the effects of new heavy particles are encoded in the Wilson coefficients of higher-dimensional operators. Within the SMEFT, we have calculated the $\mathcal{O}(\lambda)$ corrections to the $pp \to Vh$ and $pp \to jjh$ amplitudes that arise from insertions of the operator $O_6 = -\lambda \left(H^\dagger H\right)^3$ into 1-loop Feynman diagrams. We have supplemented this calculation by a computation of the $\mathcal{O}(\lambda)$ corrections to the partial decay widths of the Higgs boson in $h \to f\bar{f}$, $h \to VV$, $h \to gg$ and $h \to \gamma\gamma$. By combining both calculations we are able to derive the full $\mathcal{O}(\lambda)$ corrections to all phenomenological relevant vector boson mediated Higgs signal strengths.

To obtain accurate predictions for the $pp \to Vh$ and $pp \to jjh$ our MC simulations include QCD corrections up to NNLO. We have studied the impact of a modified h^3 vertex on the inclusive cross sections and the most important kinematic distributions in Vh

and VBF Higgs production. The dependencies of the inclusive production cross sections on $\bar{c}_6$ turn out to be process dependent and slightly stronger in the Vh channels than in VBF Higgs production. Since the $\mathcal{O}(\lambda)$ corrections to the VVh vertex depend in a non-trivial way on the external 4-momenta, the $\bar{c}_6$ dependence is also sensitive to the kinematic configurations of the final state under consideration. Our study of kinematic distributions in $pp \to Vh$ and $pp \to jjh$ shows that the shapes of the transverse momentum or invariant mass spectra in these channels are sensitive to both the size and sign of $\bar{c}_6$. However a more detailed analysis than the one performed in our article is required to determine to which extent differential information in Vh and VBF Higgs production can be used to improve the constraints on $\bar{c}_6$ that can be derived using inclusive rates. We plan to return to this question in future work.

Under the assumption that $\bar{c}_6$ is the only Wilson coefficient that obtains a non-zero correction in the SMEFT, we have then studied the sensitivity of present and future LHC measurements of Vh and VBF Higgs production to a modified h^3 interaction. We have first demonstrated that the constraint on $\bar{c}_6$ that follows from a combination of the LHC Run I measurements of signal strengths in Vh and VBF Higgs production are slightly more stringent than the limit obtained from double-Higgs production using Run I data. In the case of the HL-LHC with $3\,\text{ab}^{-1}$ of integrated luminosity, we have furthermore found that it should be possible to improve the present bound by a factor of at least 1.7. As a result indirect determinations of $|\bar{c}_6| \lesssim 9$ based on Vh and VBF Higgs production data alone should be possible. This conservative limit is not significantly weaker than the bound obtained by the ATLAS sensitivity study [23] from double-Higgs production at the HL-LHC.

Further improvements of the constraints on the trilinear Higgs coupling are possible by combining the signal strength measurements in $pp \to Vh$ and $pp \to jjh$ with those in $gg \to h$ [30, 31] and $pp \to t\bar{t}h$ [31]. The indirect probes of the trilinear Higgs coupling studied here and in [30, 31] hence provide information that is complementary to the direct determinations of λ through $pp \to hh$ production. Since the indirect and direct tests constrain different linear combinations of effective operators in the SMEFT, we believe that it is crucial to combine all available information on the h^3 coupling in the form of a global fit to fully exploit the potential of the HL-LHC. We look forward to further theoretical but also experimental investigations in this direction.

Acknowledgments

We thank Alexander Karlberg for providing optimised routines for the VBF $h + 3\,\text{jets}$ phase space and matrix elements. We are grateful to Chris Hays for helpful discussions and correspondence concerning the experimental precision that measurements of Vh and VBF Higgs production may reach at the HL-LHC and to Matthew McCullough for valuable feedback concerning his publication [28]. WB, UH and GZ have been partially supported by the ERC grant 614577 "HICCUP — High Impact Cross Section Calculations for Ultimate Precision", while the research of MG has been funded by the STFC consolidated grant ST/L000431/1. UH would like to thank the CERN Theoretical Physics Department for

continued hospitality and support. UH and GZ are finally grateful to the MITP in Mainz for its hospitality and its partial support during the initial phase of this work.

References

[1] The ATLAS and CMS Collaborations, ATLAS-CONF-2015-044.

[2] E. W. N. Glover and J. J. van der Bij, Nucl. Phys. B **309**, 282 (1988).

[3] T. Plehn, M. Spira and P. M. Zerwas, Nucl. Phys. B **479**, 46 (1996) [Erratum-ibid. B **531**, 655 (1998)] [hep-ph/9603205].

[4] S. Dawson, S. Dittmaier and M. Spira, Phys. Rev. D **58**, 115012 (1998) [hep-ph/9805244].

[5] A. Djouadi, W. Kilian, M. Mühlleitner and P. M. Zerwas, Eur. Phys. J. C **10**, 45 (1999) [hep-ph/9904287].

[6] D. de Florian and J. Mazzitelli, Phys. Rev. Lett. **111**, 201801 (2013) [arXiv:1309.6594 [hep-ph]].

[7] J. Grigo, J. Hoff, K. Melnikov and M. Steinhauser, Nucl. Phys. B **875**, 1 (2013) [arXiv:1305.7340 [hep-ph]].

[8] S. Borowka, N. Greiner, G. Heinrich, S. P. Jones, M. Kerner, J. Schlenk, U. Schubert and T. Zirke, Phys. Rev. Lett. **117**, no. 1, 012001 (2016) Erratum: [Phys. Rev. Lett. **117**, no. 7, 079901 (2016)] [arXiv:1604.06447 [hep-ph]].

[9] S. Borowka, N. Greiner, G. Heinrich, S. P. Jones, M. Kerner, J. Schlenk and T. Zirke, JHEP **1610**, 107 (2016) [arXiv:1608.04798 [hep-ph]].

[10] U. Baur, T. Plehn and D. L. Rainwater, Phys. Rev. D **67**, 033003 (2003) [hep-ph/0211224].

[11] U. Baur, T. Plehn and D. L. Rainwater, Phys. Rev. D **69**, 053004 (2004) [hep-ph/0310056].

[12] M. J. Dolan, C. Englert and M. Spannowsky, JHEP **1210**, 112 (2012) [arXiv:1206.5001 [hep-ph]].

[13] J. Baglio, A. Djouadi, R. Gröber, M. M. Mühlleitner, J. Quevillon and M. Spira, JHEP **1304**, 151 (2013) [arXiv:1212.5581 [hep-ph]].

[14] A. J. Barr, M. J. Dolan, C. Englert and M. Spannowsky, Phys. Lett. B **728**, 308 (2014) [arXiv:1309.6318 [hep-ph]].

[15] M. J. Dolan, C. Englert, N. Greiner and M. Spannowsky, Phys. Rev. Lett. **112**, 101802 (2014) [arXiv:1310.1084 [hep-ph]].

[16] A. Papaefstathiou, L. L. Yang and J. Zurita, Phys. Rev. D **87**, no. 1, 011301 (2013) [arXiv:1209.1489 [hep-ph]].

[17] F. Goertz, A. Papaefstathiou, L. L. Yang and J. Zurita, JHEP **1306**, 016 (2013) [arXiv:1301.3492 [hep-ph]].

[18] P. Maierhöfer and A. Papaefstathiou, JHEP **1403**, 126 (2014) [arXiv:1401.0007 [hep-ph]].

[19] D. E. Ferreira de Lima, A. Papaefstathiou and M. Spannowsky, JHEP **1408**, 030 (2014) [arXiv:1404.7139 [hep-ph]].

[20] C. Englert, F. Krauss, M. Spannowsky and J. Thompson, Phys. Lett. B **743**, 93 (2015) [arXiv:1409.8074 [hep-ph]].

[21] T. Liu and H. Zhang, arXiv:1410.1855 [hep-ph].

[22] F. Goertz, A. Papaefstathiou, L. L. Yang and J. Zurita, JHEP **1504**, 167 (2015) [arXiv:1410.3471 [hep-ph]].

[23] ATLAS Collaboration, ATL-PHYS-PUB-2014-019.

[24] A. Azatov, R. Contino, G. Panico and M. Son, Phys. Rev. D **92**, no. 3, 035001 (2015) [arXiv:1502.00539 [hep-ph]].

[25] A. Carvalho, M. Dall'Osso, T. Dorigo, F. Goertz, C. A. Gottardo and M. Tosi, JHEP **1604**, 126 (2016) [arXiv:1507.02245 [hep-ph]].

[26] ATLAS Collaboration, ATL-PHYS-PUB-2015-046.

[27] F. Kling, T. Plehn and P. Schichtel, Phys. Rev. D **95**, no. 3, 035026 (2017) [arXiv:1607.07441 [hep-ph]].

[28] M. McCullough, Phys. Rev. D **90**, no. 1, 015001 (2014) Erratum: [Phys. Rev. D **92**, no. 3, 039903 (2015)] [arXiv:1312.3322 [hep-ph]].

[29] C. Shen and S. h. Zhu, Phys. Rev. D **92**, no. 9, 094001 (2015) [arXiv:1504.05626 [hep-ph]].

[30] M. Gorbahn and U. Haisch, JHEP **1610**, 094 (2016) [arXiv:1607.03773 [hep-ph]].

[31] G. Degrassi, P. P. Giardino, F. Maltoni and D. Pagani, JHEP **1612**, 080 (2016) [arXiv:1607.04251 [hep-ph]].

[32] J. Elias-Miró, C. Grojean, R. S. Gupta and D. Marzocca, JHEP **1405**, 019 (2014) [arXiv:1312.2928 [hep-ph]].

[33] J. Elias-Miró, J. R. Espinosa, E. Masso and A. Pomarol, JHEP **1308**, 033 (2013) [arXiv:1302.5661 [hep-ph]].

[34] E. E. Jenkins, A. V. Manohar and M. Trott, JHEP **1310**, 087 (2013) [arXiv:1308.2627 [hep-ph]].

[35] E. E. Jenkins, A. V. Manohar and M. Trott, JHEP **1401**, 035 (2014) [arXiv:1310.4838 [hep-ph]].

[36] R. Alonso, E. E. Jenkins, A. V. Manohar and M. Trott, JHEP **1404**, 159 (2014) [arXiv:1312.2014 [hep-ph]].

[37] T. Hahn, Comput. Phys. Commun. **140**, 418 (2001) [hep-ph/0012260].

[38] T. Hahn and M. Perez-Victoria, Comput. Phys. Commun. **118**, 153 (1999) [hep-ph/9807565].

[39] A. Grau, G. Panchieri and R. J. N. Phillips, Phys. Lett. B **251**, 293 (1990).

[40] M. Gorbahn and U. Haisch, in preparation.

[41] O. Brein, A. Djouadi and R. Harlander, Phys. Lett. B **579**, 149 (2004) [hep-ph/0307206].

[42] G. Ferrera, M. Grazzini and F. Tramontano, Phys. Rev. Lett. **107**, 152003 (2011) [arXiv:1107.1164 [hep-ph]].

[43] G. Ferrera, M. Grazzini and F. Tramontano, JHEP **1404**, 039 (2014) [arXiv:1312.1669 [hep-ph]].

[44] G. Ferrera, M. Grazzini and F. Tramontano, Phys. Lett. B **740**, 51 (2015) [arXiv:1407.4747 [hep-ph]].

[45] O. Brein, R. Harlander, M. Wiesemann and T. Zirke, Eur. Phys. J. C **72**, 1868 (2012) [arXiv:1111.0761 [hep-ph]].

[46] J. M. Campbell, R. K. Ellis and C. Williams, JHEP **1606**, 179 (2016) [arXiv:1601.00658 [hep-ph]].

[47] R. Boughezal, J. M. Campbell, R. K. Ellis, C. Focke, W. Giele, X. Liu, F. Petriello and C. Williams, [arXiv:1605.08011 [hep-ph]].

[48] T. Han, G. Valencia and S. Willenbrock, Phys. Rev. Lett. **69**, 3274 (1992) [hep-ph/9206246].

[49] P. Bolzoni, F. Maltoni, S. O. Moch and M. Zaro, Phys. Rev. Lett. **105**, 011801 (2010) [arXiv:1003.4451 [hep-ph]].

[50] P. Bolzoni, F. Maltoni, S. O. Moch and M. Zaro, Phys. Rev. D **85**, 035002 (2012) [arXiv:1109.3717 [hep-ph]].

[51] M. Cacciari, F. A. Dreyer, A. Karlberg, G. P. Salam and G. Zanderighi, Phys. Rev. Lett. **115**, no. 8, 082002 (2015) [arXiv:1506.02660 [hep-ph]].

[52] F. A. Dreyer and A. Karlberg, Phys. Rev. Lett. **117**, no. 7, 072001 (2016) [arXiv:1606.00840 [hep-ph]].

[53] P. Nason and C. Oleari, JHEP **1002**, 037 (2010) [arXiv:0911.5299 [hep-ph]].

[54] W. L. van Neerven and A. Vogt, Nucl. Phys. B **568**, 263 (2000) [hep-ph/9907472].

[55] W. L. van Neerven and A. Vogt, Nucl. Phys. B **588**, 345 (2000) [hep-ph/0006154].

[56] W. L. van Neerven and E. B. Zijlstra, Phys. Lett. B **272**, 127 (1991).

[57] E. B. Zijlstra and W. L. van Neerven, Nucl. Phys. B **383**, 525 (1992).

[58] E. B. Zijlstra and W. L. van Neerven, Phys. Lett. B **297**, 377 (1992).

[59] G. P. Salam and J. Rojo, Comput. Phys. Commun. **180**, 120 (2009) [arXiv:0804.3755 [hep-ph]].

[60] B. Jäger, F. Schissler and D. Zeppenfeld, JHEP **1407**, 125 (2014) [arXiv:1405.6950 [hep-ph]].

[61] T. Figy, V. Hankele and D. Zeppenfeld, JHEP **0802**, 076 (2008) [arXiv:0710.5621 [hep-ph]].

[62] J. Alwall *et al.*, JHEP **1407**, 079 (2014) [arXiv:1405.0301 [hep-ph]].

[63] R. K. Ellis and G. Zanderighi, JHEP **0802**, 002 (2008) [arXiv:0712.1851 [hep-ph]].

[64] S. Carrazza, R. K. Ellis and G. Zanderighi, Comput. Phys. Commun. **209**, 134 (2016) [arXiv:1605.03181 [hep-ph]].

[65] J. Butterworth *et al.*, J. Phys. G **43**, 023001 (2016) [arXiv:1510.03865 [hep-ph]].

[66] LHC Higgs Cross Section Working Group, CERN report 4, https://twiki.cern.ch/twiki/bin/view/LHCPhysics/CERNYellowReportPageBR

[67] M. Cacciari, G. P. Salam and G. Soyez, JHEP **0804**, 063 (2008) [arXiv:0802.1189 [hep-ph]].

[68] M. Cacciari, G. P. Salam and G. Soyez, Eur. Phys. J. C **72**, 1896 (2012) [arXiv:1111.6097 [hep-ph]].

[69] ATLAS Collaboration, ATLAS-CONF-2016-049.

[70] R. Gröber, M. Mühlleitner, M. Spira and J. Streicher, JHEP **1509**, 092 (2015) [arXiv:1504.06577 [hep-ph]].

[71] See M. Spira's webpage http://tiger.web.psi.ch/hpair/

[72] G. Aad *et al.* [ATLAS Collaboration], Phys. Rev. Lett. **114**, no. 8, 081802 (2015) [arXiv:1406.5053 [hep-ex]].

[73] G. Aad *et al.* [ATLAS Collaboration], Eur. Phys. J. C **75**, no. 9, 412 (2015) [arXiv:1506.00285 [hep-ex]].

[74] G. Aad *et al.* [ATLAS Collaboration], Phys. Rev. D **92**, 092004 (2015) [arXiv:1509.04670 [hep-ex]].

[75] ATLAS Collaboration, ATL-PHYS-PUB-2014-011

[76] ATLAS Collaboration, ATL-PHYS-PUB-2014-012

[77] ATLAS Collaboration, ATL-PHYS-PUB-2014-016

[78] ATLAS Collaboration, ATL-PHYS-PUB-2014-018

[79] ATLAS Collaboration, ATL-PHYS-PUB-2016-008

[80] CMS Collaboration, arXiv:1307.7135.

[81] C. Boddy, S. Farrington and C. Hays, Phys. Rev. D **86**, 073009 (2012) [arXiv:1208.0769 [hep-ph]].

[82] ATLAS Collaboration, CERN-LHCC-2015-020